ELSEVIER

Nuclear Instruments and Methods in Physics Research A 449 (2000) 461–477

NUCLEAR INSTRUMENTS & METHODS IN PHYSICS RESEARCH Section A

www.elsevier.nl/locate/nima

Results from a new combined test of an electromagnetic liquid argon calorimeter with a hadronic scintillating-tile calorimeter

S. Akhmadaliev[a], F. Albiol[b], P. Amaral[c], G. Ambrosini[d], A. Amorim[c], K. Anderson[e], M.L. Andrieux[f], B. Aubert[g], E. Augé[h], F. Badaud[i], L. Baisin[d], F. Barreiro[j], G. Battistoni[k], A. Bazan[g], K. Bazizi[l], C. Bee[m], J. Belorgey[n], A. Belymam[o], D. Benchekroun[o], S. Berglund[p], J.C. Berset[d], G. Blanchot[r], A. Bogush[s], C. Bohm[p], V. Boldea[q], W. Bonivento[k], P. Borgeaud[n], O. Borisov[t], M. Bosman[r], N. Bouhemaid[a], D. Breton[h], P. Brette[i], C. Bromberg[u], J. Budagov[t], S. Burdin[v], L. Caloba[w], F. Camarena[b], D.V. Camin[k], B. Canton[x], M. Caprini[m], J. Carvalho[y], P. Casado[r], R. Cases[b], M.V. Castillo[b], D. Cavalli[k], M. Cavalli-Sforza[r], V. Cavasinni[v], R. Chadelas[i], M. Chalifour[n], L. Chekhtman[a], J.L. Chevalley[d], I. Chirikov-Zorin[t], G. Chlachidze[t,1], J.C. Chollet[h], M. Citterio[z], W.E. Cleland[aa], C. Clement[ab], M. Cobal[d,*], F. Cogswell[ac], J. Colas[g], J. Collot[f], S. Cologna[v], S. Constantinescu[q], G. Costa[k], D. Costanzo[v], J.-P. Coulon[h], M. Crouau[i], P. Dargent[m], F. Daudon[i], M. David[c], T. Davidek[ad], J. Dawson[ae], K. De[af], E. Delagnes[n], C. de la Taille[h], J. Del Peso[j], T. Del Prete[v], P. de Saintignon[f], B. Di Girolamo[d], B. Dinkespiller[m], S. Dita[q], F. Djama[m], J. Dodd[ag], J. Dolejsi[ad], Z. Dolezal[ad], R. Downing[ac], J.-J. Dugne[i], P.-Y. Duval[m], D. Dzahini[f], I. Efthymiopoulos[d], D. Errede[ac], S. Errede[ac], F. Etienne[m], H. Evans[e], G. Eynard[g], F. Farida[b], P. Fassnacht[d], N. Fedyakin[k], J. Fernandez De Troconiz[j], A. Ferrari[k], A. Ferrari[f], A. Ferrer[b], V. Flaminio[v], D. Fournier[h], G. Fumagalli[ah,*], E. Gallas[af], G. Garcia[j], M. Gaspar[w], F. Gianotti[d], O. Gildemeister[d], V. Glagolev[t], V. Glebov[l], A. Gomes[c], V. Gonzalez[b], S. Gonzalez De La Hoz[b], A. Gordeev[z], H.A. Gordon[z], V. Grabsky[ai], E. Grauges[r], Ph. Grenier[i], H. Hakopian[ai], M. Haney[ac], C. Hebrard[i], A. Henriques[d], F. Henry-Couannier[m], L. Hervas[d],

* Corresponding author. Tel.: +41-22-767-1236; fax: +41-22-767-8850.

E-mail address: cobal@atlas.cern.ch (M. Cobal).

[1] On leave from HEPI, Tbisili State University, Georgia.

* Deceased.

PII: S0168-9002(00)00153-4

E. Higon[b], S. Holmgren[p], J.Y. Hostachy[f], A. Hoummada[o], M. Huet[n], J. Huston[u], D. Imbault[x], Yu. Ivanyushenkov[r], Y. Jacquier[h], S. Jezequel[g], E. Johansson[p], K. Jon-And[p], R. Jones[d], A. Juste[r], S. Kakurin[t], P. Karst[m], A. Karyukhin[aj], Yu. Khokhlov[aj], J. Khubua[t,1], V. Klyukhin[s], G. Kolachev[a], V. Kolomoets[t], S. Kopikov[aj], M. Kostrikov[aj], V. Kovtun[t], V. Kozlov[a], P. Krivkova[ad], V. Kukhtin[t], M. Kulagin[aj], Y. Kulchitsky[s,t], M. Kuzmin[s,t], L. Labarga[j], G. Laborie[f], D. Lacour[x], S. Lami[v], V. Lapin[aj], O. Le Dortz[x], M. Lefebvre[ak], T. Leflour[g], R. Leitner[ad], M. Leltchouk[ag], A. Le Van Suu[m], J. Li[af], C. Liapis[j], O. Linossier[g], D. Lissauer[z], F. Lobkowicz[l], M. Lokajicek[al], Yu. Lomakin[t], O. Lomakina[t], J.M. Lopez Amengual[b], J.-P. Lottin[n], B. Lund-Jensen[ab], J. Lundquist[ab], A. Maio[c], D. Makowiecki[z], S. Malyukov[i], L. Mandelli[k], B. Mansoulié[n], L. Mapelli[d], C.P. Marin[d], P. Marrocchesi[v], F. Marroquin[w], L. Martin[m], O. Martin[m], Ph. Martin[f], A. Maslennikov[a], N. Massol[g], M. Mazzanti[k], E. Mazzoni[v], F. Merritt[e], B. Michel[i], R. Miller[u], I. Minashvili[t,1], L. Miralles[r], A. Mirea[m], E. Mnatsakanian[ai], E. Monnier[m], G. Montarou[i], G. Mornacchi[d], M. Mosidze[t,1], M. Moynot[g], G.S. Muanza[i], E. Nagy[m], P. Nayman[x], S. Nemecek[al], M. Nessi[d], D. Nicod[m], S. Nicoleau[q], M. Niculescu[g,d], J.M. Noppe[h], A. Onofre[am], D. Pallin[i], D. Pantea[q], R. Paoletti[v], I.C. Park[r], G. Parrour[h], J. Parsons[ag], J. Pascual[n], A. Pereira[w], L. Perini[k], J.A. Perlas[r], P. Perrodo[g], P. Pétroff[h], J. Pilcher[e], J. Pinhao[y], H. Plothow-Besch[i], L. Poggioli[d], S. Poirot[i], L. Price[ae], Y. Protopopov[aj], J. Proudfoot[ae], O. Pukhov[t], P. Puzo[h], V. Radeka[z], D. Rahm[z], G. Reinmuth[i], J.F. Renardy[n], G. Renzoni[v], S. Rescia[z], S. Resconi[k], R. Richards[u], J.-P. Richer[h], I. Riu[r], C. Roda[v], J. Roldan[b], J. Romance[b], V. Romanov[t], P. Romero[j], N. Russakovich[t], P. Sala[k], E. Sanchis[b], H. Sanders[e], C. Santoni[i], J. Santos[c], D. Sauvage[m], G. Sauvage[g], A. Savoy-Navarro[x], L. Sawyer[af], L.-P. Says[i], A. Schaffer[h], P. Schwemling[x], J. Schwindling[n], N. Seguin-Moreau[h], W. Seidl[d], J.M. Seixas[w], B. Sellden[p], M. Seman[ag], A. Semenov[t], V. Senchishin[t], L. Serin[h], E. Shaldaev[a], A. Shchelchkov[t], M. Shochet[e], V. Sidorov[aj], J. Silva[c], V. Simaitis[ac], S. Simion[n], A. Sissakian[t], I. Soloviev[an,d], R. Snopkov[a], J. Soderqvist[ab], A. Solodkov[i], P. Sonderegger[d], K. Soustruznik[ad], F. Spano'[v], R. Spiwoks[d], R. Stanek[ae], E. Starchenko[aj], P. Stavina[ao], R. Stephens[af], S. Studenov[t], M. Suk[ad], A. Surkov[aj], I. Sykora[ao], J.P. Taguet[n], H. Takai[z], F. Tang[e], S. Tardell[p], P. Tas[ad], J. Teiger[n], F. Teubert[r], J. Thaler[ac], J. Thion[g], Y. Tikhonov[a], V. Tisserand[h], S. Tisserant[m], S. Tokar[ao], N. Topilin[t], Z. Trka[ad], M. Turcotte[af], S. Valkar[ad], M.J. Varanda[c], A. Vartapetian[ai], F. Vazeille[i], I. Vichou[r], P. Vincent[x], V. Vinogradov[t], S. Vorozhtsov[t], V. Vuillemin[d], C. Walter[n], A. White[af], M. Wielers[f], I. Wingerter-Seez[g],

H. Wolters[am], N. Yamdagni[p], G. Yarygin[t], C. Yosef[u], A. Zaitsev[aj], R. Zitoun[g], Y.P. Zolnierowski[g]

ATLAS Collaboration
(Calorimetry and Data Acquisition)

[a]*Budker Institute of Nuclear Physics, Novosibirsk, Russia*
[b]*IFIC Valencia, Spain*
[c]*LIP-Lisbon and FCUL-Univ. of Lisbon, Portugal*
[d]*Division PPE, CERN, CH-1211 Geneva 23, Switzerland*
[e]*University of Chicago, USA*
[f]*ISN, Université Joseph Fourier/CNRS-IN2P3, Grenoble, France*
[g]*LAPP, Annecy, France*
[h]*LAL, Orsay, France*
[i]*LPC Clermont-Ferrand, Université Blaise Pascal/CNRS-IN2P3, France*
[j]*Univ. Autonoma Madrid, Spain*
[k]*Milano University and INFN, Milano, Italy*
[l]*Department of Physics and Astronomy, University of Rochester, New York, USA*
[m]*CPP Marseille, France*
[n]*CEA, DSM/DAPNIA/SPP, CE Saclay, Gif-sur-Yvette, France*
[o]*Faculté des Sciences Ain Chock, Universiteé Hassan II, Casablanca, Morocco*
[p]*Stockholm University, Sweden*
[q]*Horia Hulubei National Institute for Physics and Nuclear Engineering, IFIN-HH, Bucharest, Romania*
[r]*Institut de Fisica d'Altes Energies, Universitat Autònoma de Barcelona, Spain*
[s]*Institute of Physics, National Academy of Science, Minsk, Belarus*
[t]*JINR Dubna, Russia*
[u]*Michigan State University, USA*
[v]*Pisa University and INFN, Pisa, Italy*
[w]*COPPE/EE/UFRJ, Rio de Janeiro, Brazil*
[x]*LPNHE, Universités de Paris VI et VII, France*
[y]*LIP-Lisbon and FCTUC-Univ. of Coimbra, Portugal*
[z]*Brookhaven National Laboratory, Upton, USA*
[aa]*University of Pittsburgh, Pittsburgh, Pennsylvania, USA*
[ab]*Royal Institute of Technology, Stockholm, Sweden*
[ac]*University of Illinois, Urbana, USA*
[ad]*Charles University, Prague, Czech Republic*
[ae]*Argonne National Laboratory, USA*
[af]*University of Texas at Arlington, USA*
[ag]*Nevis Laboratories, Columbia University, Irvington NY, USA*
[ah]*Pavia University and INFN, Pavia, Italy*
[ai]*Yerevan Physics Institute, Armenia*
[aj]*Institute for High Energy Physics, Protvino, Russia*
[ak]*University of Victoria, British Columbia, Canada*
[al]*Academy of Science, Prague, Czech Republic*
[am]*LIP-Lisbon and Univ. Catolica Figueira da Foz, Portugal*
[an]*PNPI, Gatchina, St. Petersburg, Russia*
[ao]*Comenius University, Bratislava, Slovak Republic*

Received 4 October 1999; accepted 14 December 1999

Abstract

A new combined test of an electromagnetic liquid argon accordion calorimeter and a hadronic scintillating-tile calorimeter was carried out at the CERN SPS. These devices are prototypes of the barrel calorimeter of the future ATLAS experiment at the LHC. The energy resolution of pions in the energy range from 10 to 300 GeV at an incident

angle θ of about 12° is well described by the expression $\sigma/E = ((41.9 \pm 1.6)\%/\sqrt{E} + (1.8 \pm 0.1)\%) \oplus (1.8 \pm 0.1)/E$, where E is in GeV. The response to electrons and muons was evaluated. Shower profiles, shower leakage and the angular resolution of hadronic showers were also studied. Results are compared with those from the previous beam test.

1. Introduction

The future ATLAS experiment [1] at the CERN Large Hadron Collider (LHC) will include in the central ('barrel') region a calorimeter system composed of two separate units: a liquid argon (LAr) electromagnetic (EM) calorimeter [2] with hermetic accordion geometry and a scintillating-tile hadronic calorimeter [3] using iron as the absorber, in which the tiles are placed perpendicular to the colliding beams. This system must be capable of identifying electrons, photons and jets, and of reconstructing their energies and angles as well as of measuring the missing transverse energy in the event. The barrel calorimeter will cover the ATLAS central region over a pseudorapidity[2] range of $|\eta| \leq 1.4$.

In this paper, the results of a new test of the electromagnetic and hadronic calorimeter prototypes in a combined setup are presented, and compared with those of a previous similar test performed in 1994 [4]. The paper is organized as follows. In Section 2 the two calorimeter prototypes are briefly described, and in Section 3 the combined test beam setup and the data selection procedure are presented. The results are discussed in Sections 4–6 for electrons, pions and muons, respectively, with special emphasis on the energy resolution of hadronic showers. Finally Section 7 contains a summary and the conclusions.

2. The calorimeter prototypes

Over the past few years, several prototypes of the two calorimeters went through a series of separate test [5–9]. In 1994, for the first time, the calorimeters were tested in a combined mode. An azimuthal sector of the ATLAS barrel calorimeter was reproduced by placing the hadronic device downstream of the EM calorimeter. A second test, with the same prototypes, has been done in 1996. The purpose of this second test was to confirm the good results obtained with the previous one, but also to evaluate the combined calorimetry resolution and linearity in the low energy region. In 1994 the non-optimal beam quality of 20 GeV pions did not allow this study.

2.1. The electromagnetic liquid argon calorimeter

The electromagnetic LAr calorimeter prototype used for this test consisted of a stack of two azimuthal modules, each one spanning 9° in azimuth and extending over 2 m along the z direction. The calorimeter structure is defined by 2.2 mm thick steel-plated lead absorbers, folded to an accordion shape and separated by 3.8 mm gaps, filled with liquid argon; the signals are collected by kapton electrodes located in the gaps. The calorimeter extends from an inner radius of 131.5 cm to an outer radius of 182.6 cm, representing (at $\eta = 0$) a total of 25 radiation lengths (X_0), or 1.22 interaction lengths (λ). The calorimeter is longitudinally segmented into three compartments of $9X_0$, $9X_0$ and $7X_0$, respectively. The $\eta \times \phi$ segmentation is 0.018×0.02 for the first two longitudinal compartments and 0.036×0.02 for the last compartment. Each read-out cell has full projective geometry in η and in ϕ.

The calorimeter was located inside a large cylindrical cryostat with 2 m internal diameter, filled with liquid argon. The cryostat was made out of a 8 mm thick inner stainless-steel vessel, isolated by 30 cm of low-density foam (Rohacell), itself protected by a 1.2 mm thick aluminum outer wall. The read-out electrodes were equipped with different

[2] In the collider reference system, which has been adopted here, the z-axis indicates the LHC beam line, the x- and y-axis the horizontal and the vertical directions, while ϕ and θ are the azimuthal and polar angle, respectively. The pseudorapidity is defined as $\eta = -\ln(\tan(\theta/2))$.

types of preamplifiers, hybrid charge-sensitive preamplifiers based on SiJFETs and monolithic GaAs MESFETs, working at LAr temperature, and warm current (0 T) preamplifiers. For part of the preamplifiers, bigain shapers were used which had a peaking time of 40 ns. The signal-to-energy conversion factor was obtained using electron beams of different energies. More details about this prototype can be found in Refs. [1,5–8]. The beam incidence angle was near 12° (in 1994 it was around 11°), and the impact point was close to the center of the calorimeter face to avoid side leakage. This point is in the region equipped with Si double-gain type preamplifiers.

For most of the analysis described in this paper only part of the calorimeter was used, namely a matrix of 11×11 cells centred around the nominal beam spot for the first two longitudinal compartments and of 6×11 cells for the third. This corresponds to a front face of about 25×25 cm^2. A presampler was mounted in front of the EM calorimeter. The presampler has fine strips in the η direction and covers $\approx 11 \times 8$ in $\eta \times \phi$ EM cells in the region of the beam impact. It has 64 strips in η and two cells in ϕ. The active depth of liquid argon in the presampler was 10 mm and the strip spacing 3.9 mm. The mounting of the presampler was such that the low η part of the beam spot missed the presampler. Cuts were applied to remove these events.

2.2. The hadronic Tile calorimeter

The hadron calorimeter is a sampling device using steel as the absorber and scintillating tiles as the active material. The innovative feature of the design is the orientation of the tiles which are placed in planes perpendicular to the z direction; for a better sampling homogeneity the 3 mm thick scintillators are staggered in the radial direction. The tiles are separated along z by 14 mm of steel, giving a steel/scintillator volume ratio of 4.7. Wavelength shifting (WLS) fibres running radially collect light from the tiles at both of their open edges.

The hadron calorimeter prototype consists of an azimuthal stack of five modules. Each module covers $2\pi/64$ in azimuth and extends 1 m along the z direction, such that the front face covers 100×20 cm^2. The radial depth, from an inner radius of 200 cm to an outer radius of 380 cm, accounts for 8.9 λ at $\eta = 0$ ($80.5X_0$). Read-out cells are defined by grouping together a bundle of fibres into one photomultiplier (PMT). Each of the 100 cells is read out by two PMTs and is fully projective in azimuth (with $\Delta\phi = 2\pi/64 \approx 0.1$), while the segmentation along the z axis is made by grouping fibres into read-out cells spanning $\Delta z = 20$ cm ($\Delta\eta \approx 0.1$) and is therefore not projective. Each module is read out in four longitudinal segments (corresponding to about 1.5, 2, 2.5 and 3 λ at $\eta = 0$).

The gain of the PMTs was set to deliver $\simeq 6$ pC/GeV for incident electrons. The high voltage of each PMT was adjusted such that an equal response was obtained within a few percent by running a radioactive source through each scintillating tile. This procedure gives a first-pass cell intercalibration because the current induced in each PMT is proportional to its gain and to the photoelectron yield of the read-out cell. This intercalibration was further refined offline. A pulsed-laser system which illuminates each PMT by means of clear fibres was used to monitor short-term gain drifts. The PMT signal was digitized by a 12-bit charge-sensitive ADC which, in addition to a direct digital output, provided a second digital output with an internal amplification of 7.5, thereby giving an effective dynamic range of 15 bits.

More details of this prototype can be found in Refs. [1,10–13]. With respect to the previous combined beam test, a new element was present. In order to understand the energy loss in the dead material between the active part of the LAr and the Tile detectors a layer of scintillator was installed, called the midsampler. The midsampler consists of five scintillators, 20 cm $\times$ 100 cm each, fastened directly to the front face of the tile modules. The scintillator is 1 cm thick, and is readout using ten 1 mm WLS fibers on each of the long sides.

3. Experimental setup and test beam data

To approximate the ATLAS detector geometry the Tile calorimeter prototype was placed downstream of the LAr cryostat as shown in Fig. 1. To

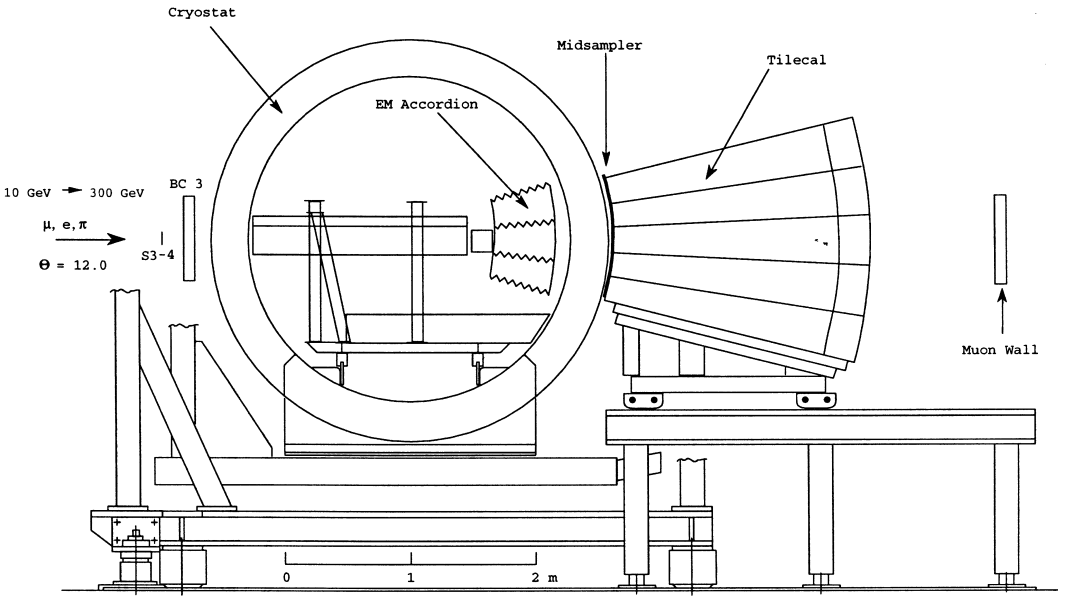

Fig. 1. Test beam setup for the combined LAr and Tile calorimeter run.

optimize the containment of hadronic showers the electromagnetic calorimeter was located as close as possible to the back of the cryostat. Early showers in the liquid argon were kept to a minimum by placing light foam material in the cryostat upstream of the EM calorimeter.

The hadronic calorimeter was placed on a table built for this test, behind and as close as possible to the LAr cryostat. Nevertheless, the distance between the active parts of the two detectors was ≈ 55 cm, a factor of two larger than in the ATLAS design configuration. The material between the two calorimeters was about $1.7X_0$, which is close to the ATLAS design value; however, the test cryostat is made of steel, with a higher Z than that of the ATLAS cryostat which will be made of aluminium.

The requirements of shower containment and space constraints implied that both the calorimeters be placed with their central axes perpendicular to their front faces at an angle of about 11° with reference to the beam. At this angle, the EM calorimeter did not point to the nominal interaction point in η; however, cell projectivity along the azimuthal direction was maintained. Due to problems during installation, an horizontal shift of the EM calorimeter occurred inside the cryostat. Using the bending magnet upstream of the setup, it was possible to recover the required conditions, by redirecting the beam with a small change in the incident angle towards the value of 12°. At 12° the two calorimeters have an active thickness of 10.3 λ (10.1 λ at $\eta = 0$, to be compared with 9.6 λ at $\eta = 0$ for the ATLAS detector).

To detect punchthrough particles, and to measure the effect of longitudinal leakage, a 'muon wall' consisting of 10 scintillator counters (each 2 cm thick) was located behind the calorimeters at a distance of about 1 m. The counters formed an array covering approximately 73 cm in the vertical and 96 cm in the horizontal directions. The muon wall counters were separated from the last tile calorimeter compartment by 0.7 λ of structural materials.

All data were taken on the H8 beam of the CERN SPS, with pion beams of 10, 20, 40, 50, 80, 100, 150, 300 GeV/c and electron beams of 20, 40, 80, 100, 150, 180 and 287 GeV/c. The electron data were used to obtain the signal-to-energy conversion factor for the EM calorimeter. Beam quality and geometry were monitored with a set of beam chambers and trigger hodoscopes placed upstream of the

LAr cryostat. The momentum bite of the beam was less than 0.5%. Single-track pion events were selected offline by requiring the pulse height of the beam scintillation counters and the energy released in the presampler to be compatible with that of a single particle. Beam halo events were removed with appropriate cuts on the horizontal and vertical positions of the incoming track impact point, as measured with the two beam chambers.

A detailed study was performed to determine the noise level in the combined setup. To measure the noise independently in the two calorimeters, pedestal triggers were recorded before and after the SPS beam burst with the same rate as the particle triggers. The total noise in the read-out system is the quadratic sum of an incoherent random component (σ_{incoh}) from the electronics, and a coherent part (σ_{coh}), which may arise from various sources, like cross-talk or pick-up from external sources. Since the coherent noise is proportional to N_{ch}, which is the number of electronic channels, even small coherent noise levels may degrade the resolution significantly when relatively large numbers of read-out cells are involved as is the case here. From the pedestal trigger data the total noise for the two calorimeters was estimated to be about 1.4 GeV.

4. Electron results

Electrons were reconstructed in the EM calorimeter for two purposes: to estimate the electron response in the EM section for the evaluation of the e/h ratio, and to check the energy resolution and linearity. To separate electrons from muons and hadrons, cuts were applied demanding a signal in the EM calorimeter compatible with electrons.

4.1. Energy resolution

To reduce the contribution of the electronic noise, the smallest possible cluster (normally 3×3 cells in $\eta\times\phi$) must be used. In the present case, however, due to the non-pointing setup of the beam, the energy leakage at the cluster boundary in η, depends on the longitudinal development of the shower as well as on the η coordinate. For this reason a 7×3 cell cluster was used. The energy seen in the 7×3 cell cluster is about 94% of the total energy.

For 287.5 GeV electrons the EM response was observed to decrease with increasing signal in the last sampling. A similar decrease was seen in Monte Carlo simulations. This is interpreted as due to longitudinal leakage and corrected for by multiplying the signal from the last sampling with a fitted factor. Due to a timing difference between the calibration and the beam particle triggers, a correction factor of 0.983 for the low-gain part of the bigain shaper signals was used. This factors only affects energies above 100 GeV. Furthermore, a multiplicative factor for the presampler signal was obtained by optimizing the energy resolution. Corrections for the measured position dependence of the energy response [5] were applied at each beam energy. Fig. 2 shows the measured energy spectrum for electrons of 287.5 GeV.

The fitted energy resolution, shown in Fig. 3, corrected for a beam momentum spread of 0.3%, is

$$\frac{\sigma_{\mathrm{E}}}{E}=\frac{11.50\pm0.52\%}{\sqrt{E}}\oplus0.0\pm0.21\%\oplus\frac{0.398\pm0.064}{E},\qquad(1)$$

where E is measured in GeV. The fitted noise term, 398 ± 64 MeV, is slightly larger than the 295 MeV measured for pedestal triggers in a 7×3 cluster. The resolution is worse than previously reported in Ref. [5] ($9.99\pm0.29/\sqrt{E}\oplus0.35\pm0.04\%$) mainly at energies between 40 and 100 GeV. This is partly attributed to the fact that, for the high gain channels of the cells in the 7×3 cluster, only a limited number of valid calibration amplitudes before

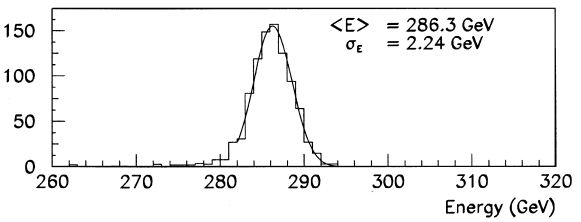

Fig. 2. The measured energy spectrum for electrons of a nominal energy 287.5 GeV.

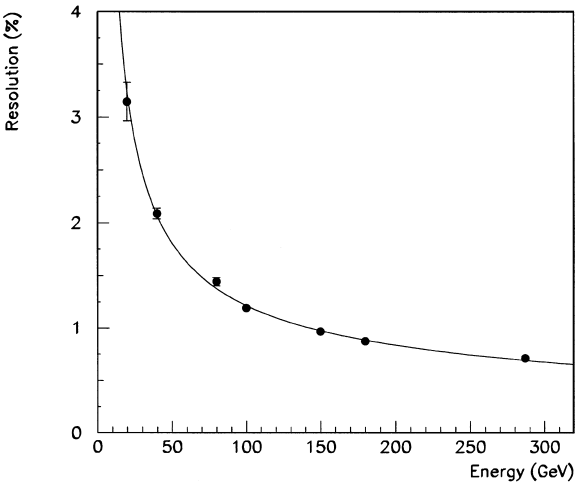

Fig. 3. The measured energy resolution for electrons in the EM calorimeter. The curve shows the fitted resolution (see text).

saturation was available. By assuming a 0.35% constant term, a fit to the energy resolution gives a sampling term of $10.96 \pm 0.15\%/\sqrt{E}$.

4.2. Response linearity

The linearity of the response in a 7×3 cell EM cluster after corrections for longitudinal leakage, signal in the presampler and measured position dependence is shown in Fig. 3, where the ratio is normalized to one at 100 GeV. The error bars are dominated by an estimate of the beam rectifier stability ($4.5\%/P$) compared to the statistical error on the average measured energy.[3] The two dashed lines in Fig. 4 shows the uncertainty on the nominal beam momentum given as

$$\frac{\Delta P}{P} = \frac{25\%}{P} \oplus 0.5\%, \tag{2}$$

where P is in GeV. The first term is related to hysteresis effects in the bending magnets, while the second term reflects calibration and geometrical uncertainties. The linearity is within errors better than 1%.

[3] P is the beam momentum.

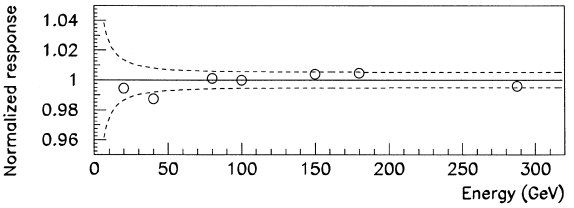

Fig. 4. The ratio of measured to nominal electron energy for 7×3 cell clusters as a function of energy. The error bars and the dashed lines are explained in the text.

5. Pion results

It is well known that the energy resolution of sampling calorimeters for hadrons is affected by several factors, among which the sampling fluctuations, the non-compensating nature of the calorimeter, and the electronic noise (at low energy) play an important role. For this combined setup, two further factors contributed to the resolution and must be taken into account in reconstructing the incident hadron energy.

1. The energy losses in the passive material between the LAr and tile calorimeters, mostly due to the outer cryostat wall.
2. The difference between the responses of the EM and tile calorimeters to the electromagnetic and hadronic components of the hadron shower, i.e. the different non-compensation of the two calorimeters.

To reconstruct the hadron energy, two different algorithms were developed [14]. The first method, referred to in the following as the 'benchmark approach', is designed to be simple. With this method the incident energy is reconstructed with a minimal number of parameters (all energy independent). The second method, the 'cell weighting technique', is inspired by the weighting technique used by the H1 experiment [15].

5.1. Energy reconstruction using a 'benchmark' approach

In the 'benchmark' algorithm, a two step procedure is adopted to reconstruct the nominal beam

energy: first, the energy of a pion is obtained as the sum of several terms, and the intervening parameters are optimized by minimizing the fractional energy resolution σ/E_0. This first-pass energy E_0 is rescaled to the nominal beam energy in a second step.

In the first step, the incident hadron energy is written as the sum of four terms.

1. The sum of the signals in the electromagnetic calorimeter, E_{em}, expressed in GeV using the calibration from electrons.
2. A term proportional to the charge deposited in the hadronic calorimeter, Q_{had}.
3. A term to account for the energy lost in the cryostat, E_{cryo}. This term is taken to be proportional to the geometric mean of the energy released in the last electromagnetic compartment (E_{em_3}) and the first hadronic compartment (Q_{had_1}). Monte Carlo studies showed agreement with this *ansatz*.
4. A negative correction term, proportional to E_{em}^2. For showers that start in the EM calorimeter, this term accounts for its non-compensating behaviour.

The first-pass energy E_0 is then

$$E_0 = E_{\mathrm{em}} + aQ_{\mathrm{had}} + b\sqrt{|E_{\mathrm{em}_3} aQ_{\mathrm{had}_1}|} + cE_{\mathrm{em}}^2 \quad (3)$$

the parameters a, b and c were determined by minimizing the fractional energy resolution of 300 GeV pions. The values of the three parameters are $a = 0.128$ GeV/pC, $b = 0.54$ and $c = -0.00054$ GeV^{-1}. It is stressed that the a parameter is not a Tile calibration constant, but has been found by minimizing the resolution. Adding the cryostat correction term E_{cryo} makes the sum $E_{\mathrm{em}} + aQ_{\mathrm{had}} + bE_{\mathrm{cryo}}$ independent of the energy in the EM calorimeter for $E_{\mathrm{em}} \leq 100$ GeV. This correction is independent of the incident pion energy. Adding the term cE_{em}^2 makes the reconstructed energy independent of the energy deposited in the electromagnetic compartment. The validity of the cryostat correction, expressed as the geometric energy mean of the last LAr sampling and the first tile calorimeter sampling, has been tested with the midsampler inserted between the cryostat and the tile calorimeter as shown in Fig. 5. In expression (3) no coefficient multiplies the LAr energy. Thus, the LAr energy scale for electrons is used as overall normalization scale.

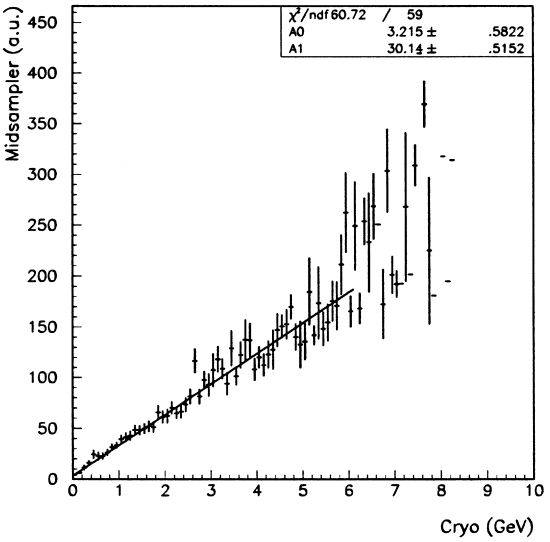

Fig. 5. Correlation between the energy released in the midsampler and the cryostat energy (Cryo) as it is defined in the benchmark expression.

This procedure minimizes the fractional energy resolution, however the reconstructed energy is systematically underestimated, due to the fact that both calorimeters are non-compensating ($e/\pi > 1$, see Ref. [9]); for this reason an additional step of rescaling is necessary. Here the aim is to compare new and old results, therefore no rescaling was applied in neither cases. The mean values E_{rec}, the resolutions σ_{rec} and the fractional resolutions $\sigma_{\mathrm{rec}}/E_{\mathrm{rec}}$ are given in Table 1 for the various beam energies. The rescaling factors vary between 1.24 and 1.55 with the beam energy.

To determine the e/π ratio for the combined setup, the knowledge of the absolute energy scale for each calorimeter is needed. The electron signal was reconstructed in the LAr calorimeter. The e/π ratio was obtained from

$$\frac{e}{\pi} = \frac{\langle E_{\mathrm{em}}^{\mathrm{e}} \rangle}{\langle E_{\mathrm{em}}^{\pi} + e_{\mathrm{Tile}} E_{\mathrm{h}}^{\pi} + E_{\mathrm{cryo}}^{\pi} \rangle}. \quad (4)$$

The denominator is similar to the benchmark formula defined above, but without the quadratic

Table 1
Mean energy, σ and fractional energy resolution for the various beam energies as obtained by using the 'benchmark' approach

Energy	E_{rec} (GeV)	σ_{rec} (GeV)	σ_{rec}/E_{rec} (%)
10 GeV	6.44 ± 0.05	1.94 ± 0.04	30.03 ± 0.72
20 GeV	14.00 ± 0.04	2.52 ± 0.04	17.52 ± 0.30
40 GeV	30.17 ± 0.08	3.70 ± 0.09	12.25 ± 0.29
50 GeV	38.29 ± 0.06	4.23 ± 0.06	11.04 ± 0.17
80 GeV	62.10 ± 0.09	5.44 ± 0.10	8.75 ± 0.16
100 GeV	77.98 ± 0.11	6.42 ± 0.10	8.23 ± 0.13
150 GeV	120.2 ± 0.13	8.04 ± 0.15	6.69 ± 0.13
300 GeV	241.66 ± 0.17	12.60 ± 0.22	5.21 ± 0.09

correction factor. E^{e}_{em} and E^{π}_{em} are the response of the LAr calorimeter to electrons and pions, E^{π}_{h} is the response of the tile calorimeter to pions and E^{π}_{cryo} is the energy loss in the cryostat. The calibration constant $e_{Tile} = 0.145$ GeV/pC is needed to achieve the correct electron energy scale in the Tile calorimeter.[4] In the case of a stand-alone calorimeter the above formula gives $e/\pi = \langle E^{e}\rangle/\langle E^{\pi}\rangle$. For the 300 GeV energy point an offset of 12.5 GeV was added to the reconstructed mean energy of the 287.5 GeV electrons.

The e/h ratio was extracted by fitting the data with the expression

$$\frac{e}{\pi} = \frac{e/h}{1 + (e/h - 1)\ 0.11 \ln E}. \quad (5)$$

Fig. 6 shows the e/π ratios for the 1996 combined data and for the 1994 combined data. The solid curve is a fit with function (5). As a result $e/h = 1.37 \pm 0.01 \pm 0.02$ was obtained, which is in good agreement with the value obtained in 1994 ($e/h = 1.35 \pm 0.04$).

The response to pions relative to electrons is seen to increase with energy as expected, because the fraction of electromagnetic energy in an hadronic shower increases with energy [16–18].

[4] The constant e_{Tile} was determined by using the response of the tile calorimeter (m.i.p. were selected in the three LAr samplings). e_{Tile} was then extracted by dividing for the $(e/\pi)_{Tile}$ measured in a stand-alone test beam.

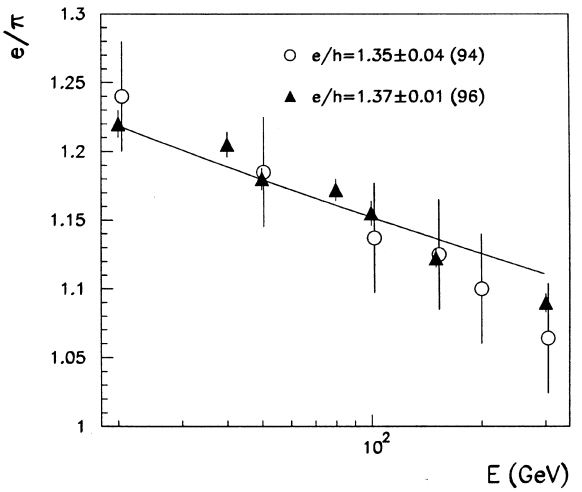

Fig. 6. Distribution of the e/π ratio versus the beam energy, fitted with expression 5. The black circles show the results for the combined 1996 setup. The open circles are the results for the combined 1994 setup.

Table 2
Mean energy, σ and fractional energy resolution for the various beam energies as obtained by using the cell weighting technique

Energy	E^{corr}_{rec} (GeV)	σ^{corr}_{rec} (GeV)	$\sigma^{corr}_{rec}/E^{corr}_{rec}$ (%)
10 GeV	9.88 ± 0.06	2.30 ± 0.05	23.28 ± 0.52
20 GeV	20.31 ± 0.04	2.91 ± 0.04	14.33 ± 0.20
40 GeV	39.96 ± 0.06	3.86 ± 0.05	9.66 ± 0.13
50 GeV	50.03 ± 0.07	4.25 ± 0.07	8.50 ± 0.14
80 GeV	79.22 ± 0.07	5.48 ± 0.06	6.92 ± 0.07
100 GeV	98.51 ± 0.1	6.09 ± 0.08	6.18 ± 0.08
150 GeV	150.24 ± 0.11	7.97 ± 0.11	5.30 ± 0.07
300 GeV	299.44 ± 0.15	12.88 ± 0.15	4.30 ± 0.05

5.2. Energy reconstruction using the cell weighting technique

The second approach to reconstruct the pion energy relies on correcting upwards the response of cells with relatively small signals, in order to equalize their response to that of cells with large (typically electromagnetic) deposited energies (Table 2). This method was succesfully applied to the combined 1994 data as described in Ref. [15]. There, an exhaustive description of the method can be found while here only its main features are described.

The total energy is reconstructed by correcting the energy in each cell of both calorimeters by

a factor (typically > 1) which is a function of the energy in each cell and of the beam energy. A correction for the energy loss in the cryostat is also applied. Thus the total energy can be expressed as:

$$E = \sum_{\text{em.cells}} W_{\text{em}}(E_{\text{cell}}, E_{\text{beam}})E_{\text{cell}} + \sum_{\text{had.cells}} W_{\text{had}}(E_{\text{cell}}, E_{\text{beam}})E_{\text{cell}} + E_{\text{cryo}} \quad (6)$$

where W_{em} and W_{had} are the weights to be determined. The energy from LAr cells is expressed in GeV while that from tile cells in pC. The cryostat term is the same as the one used for the benchmark technique described in the previous section. As a first step, the optimal weights for each beam energy are determined. To parametrize the weights as a function of the cell energies, the cell energy spectra are divided in equally populated intervals and, for each of such intervals, a weight W_i is assigned. Optimum values for the W_i are found by minimizing the energy resolution (with the constraint that the mean reconstructed energy reproduces the nominal beam energy). Finally, the weights are plotted against the mean energy released in the corresponding ith interval such that:

$$W_{\text{em}} = A_{\text{E}} + B_{\text{E}}/E_{\text{cell}} \quad (7)$$

$$W_{\text{had}} = A_{\text{H}} + B_{\text{H}}/E_{\text{cell}} \quad (8)$$

where A_{E}, B_{E}, A_{H} and B_{H} are taken from a fit and are specific for a given beam energy. The same exercise is repeated for all the available beam energies, using the same interval definition to avoid biases. As a result, a set of 4 parameters (A_{E}, B_{E}, A_{H} and B_{H}) are defined for each beam energy ($4 \times 8 = 32$ parameters).

Once the weights dependence on the cell energy has been determined, the dependence on the beam energy is studied. The A_{E}, B_{E}, A_{H} and B_{H} are further parametrized as a function of the beam energy. The total number of parameters is reduced to 8 (including the cryostat constant). To avoid any dependence on the knowledge of the beam energy, the following algorithm has been developed.

1. The beam energy was estimated as $1.24E_0$ (E_0 being the energy reconstructed with the benchmark technique) and used to evaluate the weights, instead of the true beam energy. The factor 1.24 is the one needed to rescale the calorimeter response for 300 GeV pions to the correct value.
2. The cell weighting algorithm was then applied.
3. The weights were recomputed using the energy reconstructed in the previous step.
4. This procedure was iterated until stable results were obtained.

After three iterations the reconstructed energy is stable within few tens of MeV.

5.3. Resolution and linearity

The energy resolutions (σ/E) obtained with the benchmark energy reconstruction methods are plotted in Fig. 7 as a function of $1/\sqrt{E}$. Results from the 1994 and 1996 combined beam tests are compared. A fit to the 1996 data points gives a fractional resolution of $[(59.5 \pm 2.6)\%/\sqrt{E} + (1.8 \pm 0.2)] \oplus (2.0 \pm 0.1)/E$. The sampling term is larger than that obtained with the 1994 data: $[(52.1 \pm 5.5)\%/\sqrt{E} + (1.9 \pm 0.3)] \oplus (3.2 \pm 0.4)/E$ [4]. However, there is a correlation between the noise and the sampling terms. Decreasing the noise term (owing to the 20 GeV point, which in the 1994 data had a worse resolution, probably due to

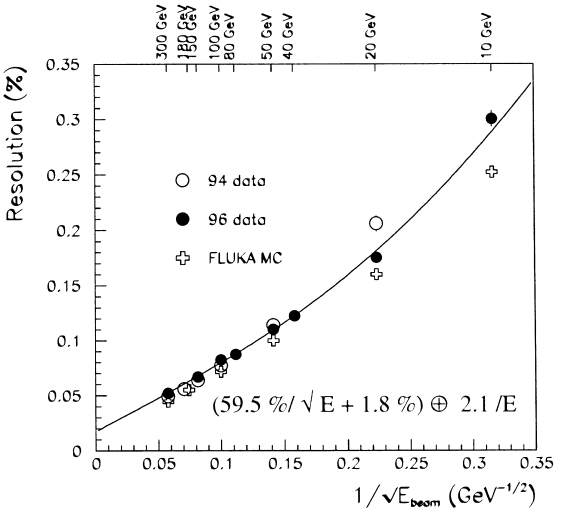

Fig. 7. Fractional energy resolution obtained with the benchmark method.

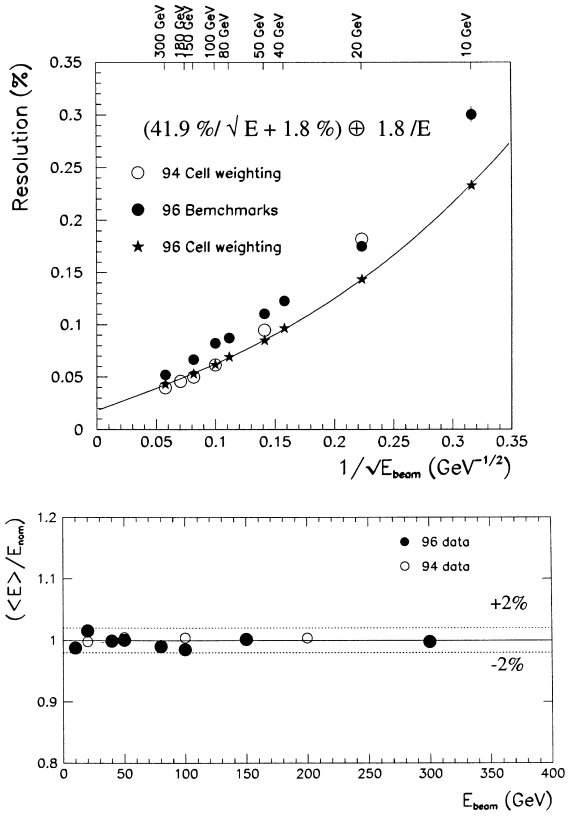

Fig. 8. Upper plot: fractional energy resolution obtained with the cell weighting technique. The results are compared with those obtained by applying the benchmark method and with the cell weighting results of 1994. Lower plot: response linearity as a function of the beam energy. The cells weighting technique was used.

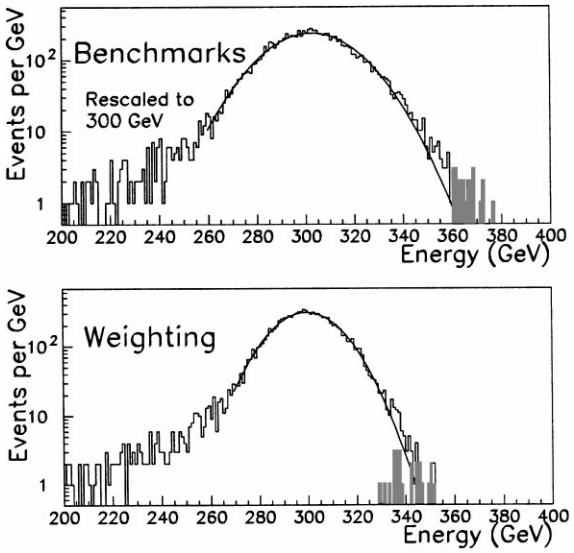

Fig. 9. Energy spectra for 300 GeV pions reconstructed with the benchmark technique (top plot) as well as with the cell weighting technique (bottom plot).

a non-optimal beam quality) results in an increase of the sampling term.

The combined setup was simulated with the standalone FLUKA [19] program. Details of the simulations have already been reported in Ref. [4]. The 10 GeV point has been added with an estimated proton contamination of 14%. The presampler has been implemented together with a clustering algorithm as similar as possible to the experimental one. Simulated data have been reconstructed with the benchmark technique, with energy independent parameters fixed by minimizing the fractional energy resolution at 300 GeV. The FLUKA data reproduce quite well the experimental values except for the 10 GeV point (Fig. 7), where, however, the result is strongly dependent on the capability of removing events with interactions in the dead material upstream of the calorimeter and the muon contamination. The fractional resolution obtained by reconstructing the energy with the cell weighting procedure is shown in Fig. 8 (upper plot). The resolution is fitted by the function $[(41.9 \pm 1.6)\%/\sqrt{E} + (1.8 \pm 0.1)\%] \oplus (1.8 \pm 0.1)/E$.

The noise term is lower and the sampling term is a little higher than those obtained from the 1994 data, as already noticed with the benchmark method. It can be concluded that the cell weighting technique improves the energy resolution obtained with a simpler approach. The linearity of the calorimeter response to pions is shown in Fig. 8 (lower plot). A comparison is made between the results obtained with the 1994 and 1996 data sets using the cell weighting technique. The response to pions is well within $\pm$ 2% over the full energy range of the data.

Fig. 9 shows the energy spectra for 300 GeV pions reconstructed with the benchmark (upper plot) and with the cell weighting (lower plot) techniques. The means of the distributions are rescaled

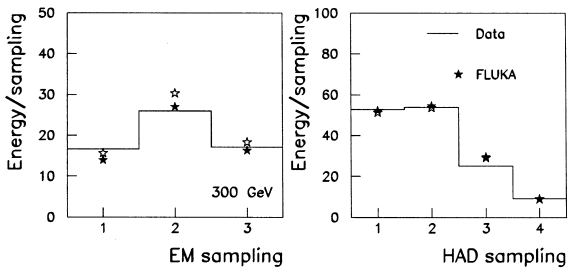

Fig. 10. Longitudinal shower profile for 300 GeV pions. The black and white stars refer to two different sets of parameters in the FLUKA Monte Carlo.

to 300 GeV. The high-energy tails are due to the intrinsic non-Gaussian characteristics of hadronic showers. After applying the benchmark energy reconstruction about 0.18% of the events are at more than 3.5σ from the mean. Most of these events disappear from the tails once the cell weighing technique is used to reconstruct the energy. The low-energy tails are mostly due to events which suffer from an incomplete longitudinal shower containment. They can be reduced by removing the events with a signal in the muon wall behind the calorimeter, as already shown in Ref. [4].

5.4. Longitudinal shower profile and angular resolution

The mean raw energy deposited in each sampling can be plotted against the calorimeter depth to obtain a representation of the shower longitudinal profile. Fig. 10 shows the longitudinal profiles for pions of 300 GeV for data and Monte Carlo. The electron scale is used for the EM calorimeter. For the tile calorimeter the calibration constant 0.145 as for the e/π calculation is used. The FLUKA results, shown for two different sets of parameters obtained by applying the benchmark energy reconstruction, are in reasonable agreement with the data in both calorimeters.

The data collected were also used to determine the angular resolution for hadronic showers. For this study, the cells in the fourth longitudinal sampling of the tile calorimeter were not used, since they only have a small amount of deposited energy. To determine the resolution in polar angle with a precision of better than the hadronic cell size (100 mrad), for each longitudinal sampling (i) the center of gravity along the horizontal axis (x^i_{CG}) in the plane of the front face of the calorimeter was measured, on an event-to-event basis:

$$x^i_{\mathrm{CG}} = \frac{\sum_{j,k} E^i_{j,k}\, x^i_k}{\sum_{j,k} E^i_{j,k}} \tag{9}$$

In the plane of the calorimeter front face, the k index runs along the horizontal axis x, and the j index runs along the vertical axis y (or angle ϕ). Therefore, $E^i_{j,k}$ is the energy deposited in cell (j,k) of the ith longitudinal sampling, and x^i_k is the x central position of the kth cell in the horizontal axis. Since the electromagnetic compartment has a projective geometry, the cell center positions are first converted from η values (in rad) to x values (in cm). The polar angle θ was determined for each event by a linear fit to the equation

$$\bar{z}^i = \tan(\theta) x^i_{\mathrm{CG}} + b \tag{10}$$

where $\bar{z}^i$ is the ith longitudinal sampling center position (along the radial z-axis) and b is an arbitrary intercept. For each energy the angular resolution σ_θ is obtained from a Gaussian fit to the reconstructed beam angle θ. The angular resolution is shown in Fig. 11 as a function of the beam energy: it is a linear function of $1/\sqrt{E}$. The fit gives: $\sigma_\theta = [(160.50 \pm 1.48)/\sqrt{E} + (8.15 \pm 0.20)]$ mrad. Averaging over all energies a mean polar angle $\bar{\theta} = (11.87 \pm 0.09)^{\circ}$ was obtained, which agrees with the nominal beam angle of about 12°. The non-pointing geometry of the setup in the η direction produces a degradation of the polar angle resolution. A better result is obtained looking at the resolution in the azimuthal angle, where one has full projectivity.

The azimuthal angle (ϕ) was reconstructed for each longitudinal sampling (i) and each event using the formula

$$\phi^i_{\mathrm{CG}} = \frac{\sum_{j,k} E^i_{j,k}\, \phi^i_j}{\sum_{j,k} E^i_{j,k}}. \tag{11}$$

As in Eq. (9), k runs over the horizontal axis, and j runs along the vertical axis. The beam hits the calorimeter at $\phi = 0$. For each event the average of the six values of ϕ^i_{CG} is calculated. Fig. 12 shows

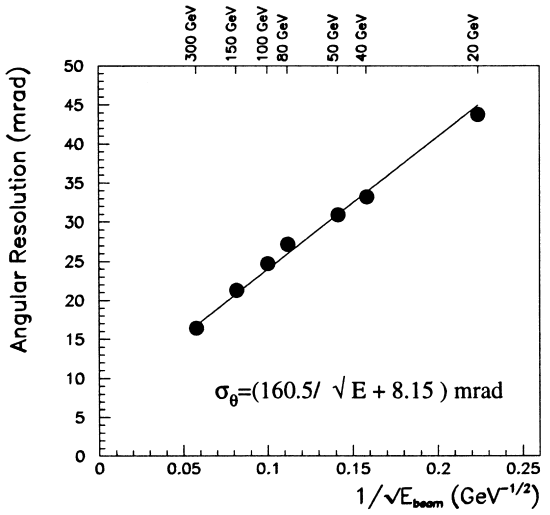

Fig. 11. Polar angular resolution σ_θ as a function of $1/\sqrt{E}$.

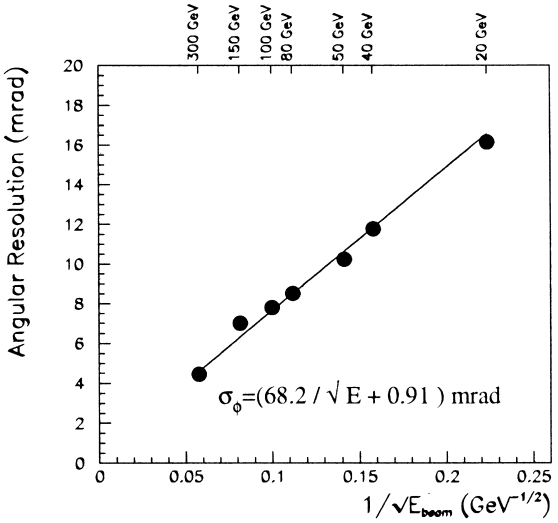

Fig. 12. Azimuthal angular resolution σ_ϕ as a function of $1/\sqrt{E}$.

σ_ϕ as a function of $1/\sqrt{E}$. The fit gives $\sigma_\phi = [(68.17 \pm 0.75)/\sqrt{E} + (0.91 \pm 0.11)]$ mrad.

5.5. Shower leakage studies

As already mentioned, in this combined calorimeter test particles incident at an angle of about 12° traverse about 11 interaction lengths, including passive materials at the back of the tile calorimeter. Punchthrough particles can be muons from π and K decays in a hadronic cascade, or charged particles (mainly soft electrons and hadrons) and neutrons from showers not fully contained in the calorimeter. For this study, pions in the range 40–300 GeV were examined [20,21].

The probability of longitudinal shower leakage was defined as the fraction of events with a signal in at least one of the muon wall counters. To be considered as a punchthrough signal, the signal Q_i in any counter must satisfy the requirement

$$Q_i > (\bar{Q}_i^{\mu} - 3\sigma_i^{\mu}). \tag{12}$$

The average ($\bar{Q}_i^{\mu}$) and sigma values (σ_i^{μ}) were determined using the most probable energy deposition and width of muons in the muon wall. Since the muon wall does not cover the whole back of the calorimeter, an evaluation of its acceptance was performed. The acceptance in 1996 has increased with respect to 1994, due to a better coverage of the calorimeter. Fig. 13 (upper plot) shows the probability of longitudinal shower leakage as a function of the beam energy. The probability is corrected for the acceptance which is around 52%. At 100 GeV this probability is about 11%. The measurements are in agreement (inside errors) with what obtained in the previous combined test. Fig. 13 (lower plot) shows the energy loss from leakage averaged over punchthrough events, defined as the difference between the mean energy values of events with and without a signal in the muon wall, for several beam energies. The energy loss for events with longitudinal leakage is about 3% at 100 GeV, and less than 2.5% at 300 GeV (Fig. 14).

6. Muon results

The tile calorimeter response to muons has been investigated for several beam energies (20 to 150 GeV). The reconstruction of a muon signal is important for several interesting physics processes at the LHC [22], and can be used for detector intercalibration as well.

Muons were extracted from the pion beams. The muon signal is small, so the noise must be treated

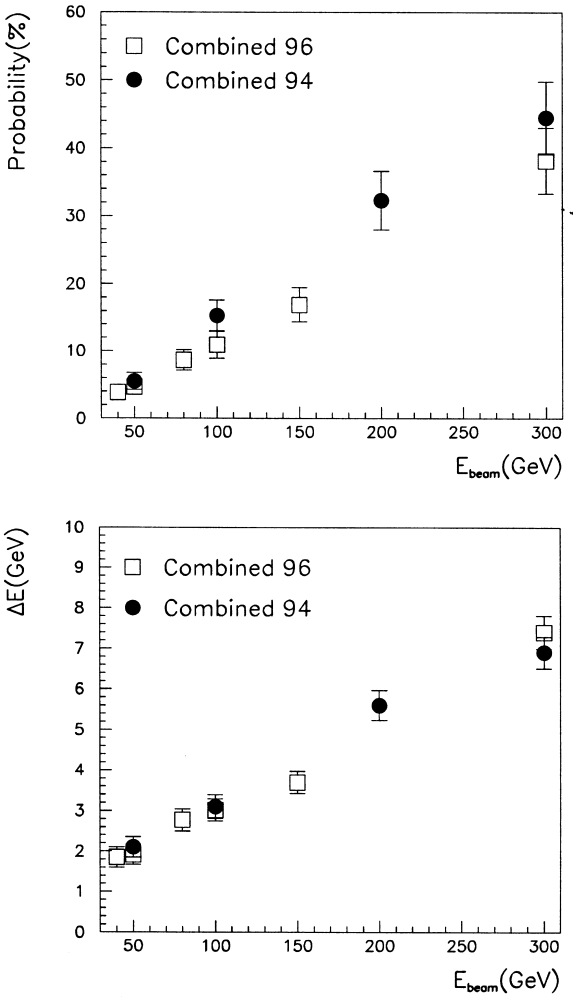

Fig. 13. Upper plot: punchthrough probability for pions. Results from the 1994 combined test beam are shown as well. Lower plot: average energy loss as a function of beam energy for events with longitudinal leakage.

carefully. For the absolute energy scale, 100 GeV pions were used, taking into account the tile calorimeter e/π ratio (see Ref. [3]).

In order to avoid summing up cells without signal, only the central modules (2,3,4) were used since the beam hits the center of module 3 in the ϕ direction. Furthermore, in each longitudinal sampling, a cell with the maximum average signal was taken as the central one, since it corresponds to the cell where the beam is supposed to enter. The central cells always belong to module 3. The other cells are

Table 3
Total tile calorimeter to muons at various energies. The MOP and FWHM values were obtained with the convolution of a Landau and a Gaussian function. The values of peak and width are those from the Landau part of the convolution

E_{beam} (GeV)	Total signal		Total noise	S/N
	MOP (GeV)	FWHM (GeV)	σ_{noise} (GeV)	
20	2.35	0.83	0.066	36.0
40	2.41	0.89	0.065	37.0
50	2.44	0.83	0.064	38.0
80	2.46	0.93	0.064	38.0
100	2.55	1.14	0.067	38.0
150	2.66	1.23	0.068	39.0

then searched for in a 3×3 cell window around the central cell. The muon signal in the hadron calorimeter has been reconstructed summing two cells from the 3×3 window with the maximum signal content in each longitudinal sampling.[5]

As the muon signal is formed summing up a pair of channels which can vary event by event, the corresponding noise has been treated as the noise sum of the respective pair of channels. The muon signal distribution is fitted with the convolution of a Landau and a Gaussian function. The most probable (MOP) values of the muon signal in the tile calorimeter are listed in Table 3. The MOP values slightly increase with the incident muon energy. The signal-to-noise ratio (S/N) is reported in the table as well.

7. Summary and conclusions

A new test of the combined electromagnetic liquid argon and the hadronic Tile-iron calorimeter prototypes of the future ATLAS experiment was carried out, using pion beams of energy 10–300 GeV. The good results obtained with the first test

[5] The full sum of 9 cells results in the same (within errors) most probable signal prediction as does the method used, but the peak is wider. However, the method used might underestimate the energy loss for muons emitting bremsstrahlung or electron–positron pairs.

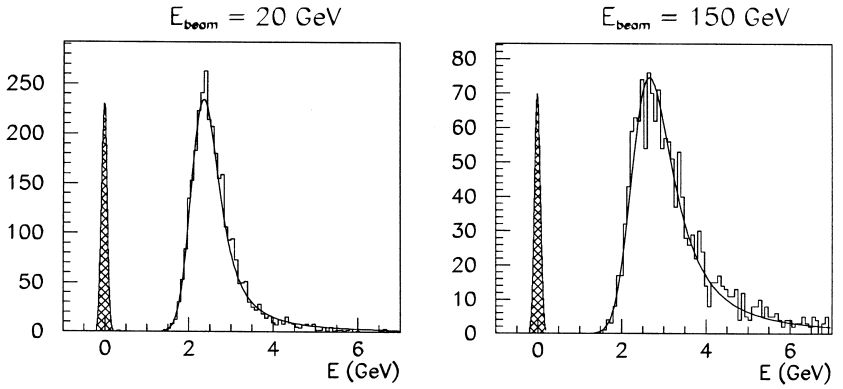

Fig. 14. The Tile calorimeter response to muons of 20 GeV (left plot) and 150 GeV (right plot). The signal was fitted using a convolution of a Landau and a Gaussian function. The hatched area corresponds to the noise distribution.

have been confirmed. The response of the combined setup to electrons and muons has been studied. Two different methods of reconstructing the hadronic beam energy were used; the best resolution is obtained using a cell weighting technique, which gives $\sigma/E = ((41.9 \pm 1.6)\%/\sqrt{E} + (1.8 \pm 0.1)\%) \oplus (1.8 \pm 0.1)/E$, where E is in GeV.

The e/h ratio of the combined prototypes was found to be $1.37 \pm 0.01 \pm 0.002$.

Energy resolutions and longitudinal profiles are well reproduced by a simulation with standalone FLUKA, with some discrepancy at 10 GeV.

The angular resolution in the ϕ direction for hadron showers was studied. The resolution can be described by the function $\sigma_\phi = (68.17 \pm 0.75)/\sqrt{E} + (0.9 \pm 0.11)$ mrad. The angular resolution in the θ direction is instead degraded, due to the non-projectivity of the calorimeter cells in the η direction. Punchthrough studies show that even after about 10 nuclear interaction lengths shower energy leakage at the highest energies is not negligible.

Acknowledgements

We sincerely thank the technical staffs of the collaborating Institutes for their important and timely contributions. Financial support is acknowledged from the funding agencies of the collaborating Institutes. Finally, we are grateful to the staff of the SPS, and in particular to K. Elsener, for the excellent beam conditions and assistance provided during our tests.

References

[1] ATLAS collaboration, Technical proposal, CERN/LHCC/94-43 LHCC/P2.
[2] ATLAS liquid argon calorimeter technical design report, CERN/LHCC/96-41.
[3] ATLAS tile calorimeter technical design report, CERN/LHCC/96-42.
[4] Z. Ajaltouni et al., Nucl. Instr. and Meth. A 387 (1997) 335.
[5] D.M. Gingrich et al., (RD3 Collaboration), Nucl. Instr. and Meth. A 364 (1995) 290.
[6] B. Aubert et al., (RD3 Collaboration), Nucl. Instr. and Meth. A 325 (1993) 118.
[7] B. Aubert et al., (RD3 Collaboration), Nucl. Instr. and Meth. A 321 (1992) 467.
[8] B. Aubert et al., (RD3 Collaboration), Nucl. Instr. and Meth. A 309 (1991) 438.
[9] F. Ariztizabal et al., (RD34 Collaboration), Nucl. Instr. and Meth. A 349 (1994) 384.
[10] F. Ariztizabal et al. (RD34 Collaboration), LRDB Status Report, CERN/LHCC 95-44.
[11] O. Gildemeister, F. Nessi-Tedaldi, M. Nessi, in: A. Ereditato (Ed.), Proceedings of the II International Conference on Calorimetry in High Energy Physics, Capri, 1991, World Scientific, Singapore, 1991.
[12] M. Bosman et al. (RD34 Collaboration), CERN/DRDC/93-3, 1993.
[13] F. Ariztizabal et al. (RD34 Collaboration), CERN/DRDC/94-66, 1994.
[14] M. Cobal et al., ATLAS Internal Note, TILECAL-NO-168, 1998.

[15] M.P. Casado, M. Cavalli Sforza, ATLAS Internal Note. TILECAL-NO-75, 1996.
[16] D.E. Groom, in: A. Ereditato (Ed.), Proceedings of the II International Conference on Calorimetry in High Energy Physics, Capri, 1991, World Scientific, Singapore, 1992.
[17] T.A. Gabriel, D.E. Groom, P.K. Job, N.V. Mokhov, G.R. Stevenson, Nucl. Instr. and Meth. A 338 (1994) 336.
[18] R. Wigmans, Nucl. Instr. and Meth. A 259 (1987) 389.
[19] A. Ferrari, P.R. Sala, The physics of high energy reactions, in: A. Gandini, G. Reffo (Eds.), Proceedings of the Workshop on Nuclear Reaction Data and Nuclear Reactors Physics, Design and Safety, International Centre for Theoretical Physics, Miramare-Trieste, Italy, 15 April–17 May 1996, World Scientific, Singapore, 1998, Also ATLAS internal note PHYS-NO-113.
[20] M. Lokajicek et al., ATLAS internal note, TILECAL-NO-63, 1995.
[21] M. Lokajicek et al., ATLAS internal note, TILECAL-NO-64, 1995.
[22] ATLAS Collaboration, Detector and physics performance technical design report, CERN/LHCC/99-15.